APPLIED MATERIALS AND TECHNOLOGY

Jamt.ejournal.unri.ac.id

Research Article

Preparation and characterization of MoS_2 thin films for thermoelectric applications using the PVD technique

Joede dos Passos*, Adhimar Flavio Oliveira, Rero Marques Rubinger

ABSTRACT: Molybdenum disulfide (MoS_2) is a two-dimensional material with electronic and thermal properties that make it promising for thermoelectric applications. This research presents the results of synthesizing and characterizing MoS_2 thin films obtained by Physical Vapor Deposition (PVD) on silicon dioxide (SiO_2) substrates. Three experimental approaches were explored to assess how changes in deposition conditions affect the material quality. In the first trial, films were formed from commercial MoS_2 powder in a sulfur-rich (S_2) atmosphere using a PVD tubular furnace. Next, water vapor (H_2O) was added to the process to observe possible improvements in material formation. Finally, silver doping was investigated, introduced during deposition to examine structural and vibrational changes in the MoS_2. The samples were characterized by Optical Microscopy (OM) and Scanning Electron Microscopy (SEM), as well as Energy Dispersive Spectroscopy (EDS), used to evaluate surface morphology and composition. X-ray Diffraction (XRD) was employed to identify the crystalline structure, while Raman Spectroscopy revealed the E_2g^1 and A_1g vibrational modes, associated with the crystallinity of the material. The results indicated that the presence of H_2O during deposition favored the growth of more ordered films, with more intense peaks in XRD and Raman spectra. On the other hand, silver doping caused vibrational changes that suggest modifications in the electronic structure of MoS_2. These findings reinforce the material's potential for use in thermoelectric devices and demonstrate that variations in synthesis conditions can significantly enhance its structural and functional properties.

Keywords: *MoS_2 thin films, Physical Vapor Deposition (PVD), Silver doping, Structural and morphological characterization, Thermoelectric applications*

1. INTRODUCTION

Molybdenum disulfide (MoS_2) is a two-dimensional semiconductor with remarkable electronic, optical, and mechanical properties, showing great promise for applications in energy conversion devices [1,2]. In its bulk form, it exhibits an indirect band gap of approximately 1.2 eV, which becomes direct and increases to about 1.8 eV when reduced to a few atomic layers, resulting in intense photoluminescence [3]. This band gap transition, combined with its high absorption in the infrared region, also favors the use of MoS_2 in biomedical and photothermal applications [4,5].

For the growth of MoS_2 thin films, several techniques have been explored, such as micromechanical exfoliation, ionic intercalation, liquid-phase ultrasonication, and Physical Vapor Deposition (PVD) [6]. PVD stands out for enabling the controlled growth of nanometric films with high purity and no external contamination, in addition to allowing the tuning of parameters such as temperature, pressure, and deposition rate for optimizing the material's properties.

Recent studies have shown that the physical and chemical characteristics of MoS_2 are strongly influenced by synthesis conditions and the surrounding chemical environment during deposition. Parameters such as sulfur partial pressure, substrate temperature, and the presence of oxidizing or reducing agents can significantly modify crystal orientation, defect concentration, and electronic behavior [7,8]. In particular,

OPEN ACCESS

Affiliation
Universidade Federal de Itajubá, Av BPS, 1303, Itajubá, 37500-903, Brasil

***Correspondence**
Email: d2019017104@unifei.edu.br

ORCID
Passos, J.: 0009-0004-4291-4350
Oliveira, A., F.: 0000-0003-2586-7359
Rubinger, R., M.: 0000-0003-1718-9658

Received: November 08, 2025
Revised: November 30, 2025
Accepted: December 08, 2025

How to cite: Passos, J., Oliveira, A., F., N., Rubinger, R., M., (2025). Preparation and characterization of MoS_2 thin films for thermoelectric applications using the PVD technique. *Journal of Applied Materials and Technology*, 7(2), 49–57. https://doi.org/10.31258/Jamt.7.2.49-57.

the incorporation of oxygen or hydroxyl species, often introduced through residual H_2O, can lead to the formation of Mo–O bonds, altering the band structure and enhancing catalytic or photothermal performance [9,10].

Moreover, doping strategies have emerged as an effective route to tune the electronic and thermoelectric properties of MoS_2. The introduction of metallic dopants such as Ag, Au, or Pt can modulate carrier concentration, reduce thermal conductivity, and improve charge transport by introducing localized states within the band gap [11,12]. Silver (Ag) doping, in particular, has been associated with enhanced Seebeck coefficients and electrical conductivity, making Ag–MoS_2 composites promising candidates for thermoelectric and optoelectronic applications [13,14].

Considering the versatility of MoS_2 and the need to understand the impact of synthesis conditions on its properties, this research proposes an experimental approach to investigate the effects of H_2O presence and silver (Ag) doping on the morphology, structure, and vibrational characteristics of MoS_2 films obtained via Physical Vapor Deposition (PVD). The ultimate goal is to identify and enhance material properties of interest for application in advanced energy conversion devices, such as thermoelectric generators.

Although previous studies have investigated the role of sulfur availability, oxygen contamination, or metal dopants independently in MoS_2 thin-film growth, the combined influence of residual H_2O during PVD deposition and Ag incorporation has not yet been systematically explored. Residual water vapor can act simultaneously as an oxidizing and transport-assisting species, altering Mo–S bond stability and favoring the formation of secondary phases such as MoO_2. At the same time, Ag doping is known to modify charge carrier concentration, local strain, and defect density in layered chalcogenides. However, no prior work has evaluated how these two factors interact during PVD growth, nor how this interplay affects the crystallinity, oxidation pathways, and functional properties of MoS_2 thin films. In this context, the present study provides the first integrated analysis of MoS_2 films grown under controlled H_2O environments with and without Ag doping, contributing new insight into how moisture and metal dopants jointly modulate the structural and thermoelectric behavior of PVD-grown MoS_2.

2. EXPERIMENTAL

The substrates were obtained from a silicon wafer (100) supplied by Sigma-Aldrich and cut into pieces of approximately 10 mm^2 using a diamond scribe. The samples then underwent a thorough cleaning procedure, beginning with immersion in acetone and placement in an ultrasonic bath. During sonication, the substrates were kept for 15 minutes to remove surface contaminants such as dust and organic residues. Subsequently, they were rinsed in isopropyl alcohol and then in deionized water. After cleaning, the substrates were dried with a high-purity nitrogen jet, ensuring they were properly sanitized and ready for the next processing steps.

The cleaned samples were then placed in a furnace (model FDG 3P-S), which was heated to 900 °C and maintained at that temperature for 10 hours. One of the samples was kept as a reference substrate for reflectance calibration. Reflectance measurements were performed on both the oxidized samples and the reference sample using a Stellarnet UV–VIS–NIR spectrometer, covering the wavelength range from 200 nm to 1080 nm. A halogen lamp served as the light source, and an aluminum mirror was used for calibration. The obtained reflectance spectra were analyzed to determine the optical properties of the samples. From these measurements, differences between the oxidized and reference samples were identified, allowing estimation of the SiO_2 layer thickness formed by thermal oxidation.

For the growth of the MoS_2 film without the presence of distilled water (sample J1), the SiO_2 substrate was placed inside the Physical Vapor Deposition (PVD) furnace (Figure 1). Ten grams of sulfur (Êxodo Científica) and 10 g of MoS_2 (Sigma-Aldrich) were weighed, placed in separate crucibles, and introduced into the system. The substrate was positioned in the downstream region of the tubular furnace, where the temperature reached 800 °C. The crucible containing sulfur was positioned outside the furnace, inside a beaker placed on a DUBAI magnetic heater, connected by a polyurethane hose (PU Rodo Azul, 6 mm). Nitrogen (N_2) was used as the carrier gas, passing through the sulfur container and directed toward the end of the tubular furnace. A continuous N_2 flow was maintained at a pressure of 75 Torr and a rate of 70 sccm. The total growth process lasted 1.8 hours, reaching a maximum temperature of 1000 °C, which was held for 5 minutes. This procedural flow, summarized in Figure 2, provides a clear overview of the key stages required for obtaining MoS_2 thin films under the different synthesis conditions evaluated in this work.

The procedures for the other two samples followed similar steps, with specific variations: in one case, a crucible containing distilled water was added together with the sulfur source; in the other, a crucible containing silver nitrate ($AgNO_3$) was placed inside the furnace tube at the 960 °C zone to enable silver doping of the MoS_2 film.

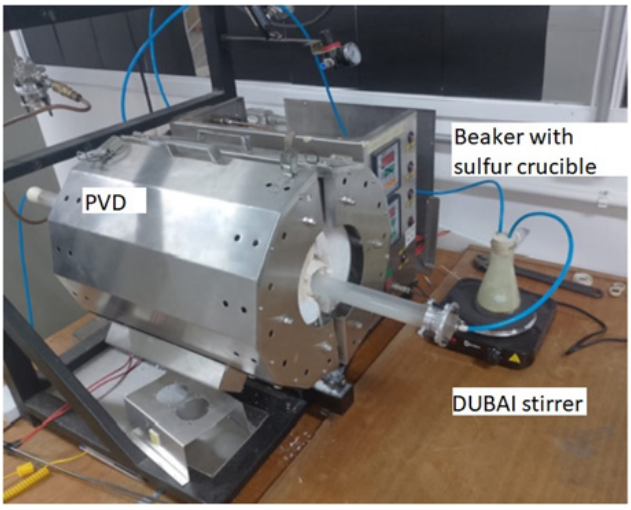

Figure 1. Flowchart Experimental setup for MoS_2 synthesis using Physical Vapor Deposition (PVD). The system includes a tubular furnace, a quartz tube connected to a beaker containing the sulfur crucible, and a DUBAI magnetic stirrer used for sulfur vapor control.

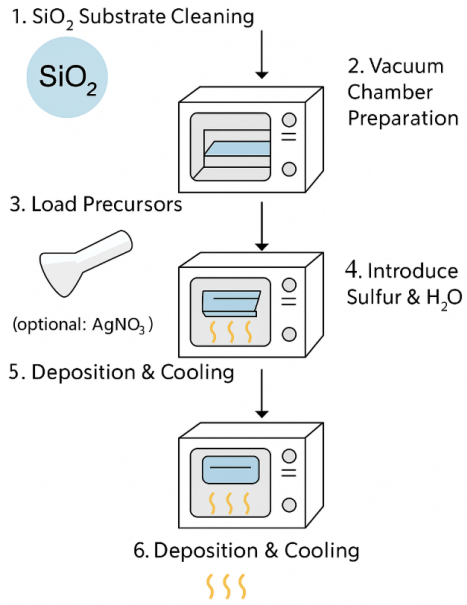

Figure 2. Schematic representation of the synthesis procedure used for the preparation of MoS_2 thin films by Physical Vapor Deposition (PVD). The diagram illustrates the sequential steps of the process, including substrate cleaning, vacuum chamber preparation, precursor loading, introduction of sulfur and optional $AgNO_3$, and the deposition/cooling stage inside the tubular furnace.

Chemical and structural analyses were performed by X-ray diffraction (XRD) using a PANalytical X'Pert PRO diffractometer equipped with Cu Kα radiation. Scans were carried out over a 2θ range from 5° to 80°, with a step size of 0.02° and a counting time of 2 s per step. Raman spectroscopy analyses were performed using a WITec Alpha300R confocal Raman spectrometer with an excitation wavelength of 532 nm and a 100× objective lens. The Raman spectra were acquired with an integration time of 10 s and 5 accumulations. The excitation laser power was kept below 1 mW to prevent local heating or damage to the samples.

3. RESULT AND DISCUSSION

To determine the thickness of the SiO_2 film grown on a Si substrate, reflectance measurements were performed, and the data were subsequently fitted using the three-layer thin-film model [15]. The average thickness obtained for the films was 280 ± 10 nm, which is consistent with typical oxide growth under the reported oxidation parameters. The reproducibility of this value confirms the thermal stability and surface uniformity of the SiO_2 substrate used for subsequent MoS_2 deposition.

The X-ray diffraction (XRD) analysis of MoS_2 thin films synthesized under different conditions (samples J1, J2, and J3) is shown in Figure 3. All diffraction patterns display the characteristic reflections of hexagonal 2H–MoS_2, with the most intense peak located at 2θ ≈ 14.4°, corresponding to the (002) plane, indicative of the material's layered structure [16]. The significantly higher intensity and narrower full width at half maximum (FWHM) of this peak in sample J2, grown in the presence of H_2O vapor, suggests improved crystallinity and enhanced layer ordering. This behavior is consistent with reports that water vapor facilitates sulfur transport and increases surface mobility during growth, promoting higher-quality layered films [17].

In contrast, the XRD pattern of sample J1 (synthesized without H_2O) exhibits additional reflections that do not belong to the MoS_2 phase. Specifically, weak but detectable peaks at approximately 2θ ≈ 26.0° and 37.3° were identified and assigned to the (110) and (211) planes of monoclinic MoO_2 (JCPDS 32-0671), respectively. These reflections indicate partial oxidation of MoS_2, likely caused by limited sulfur availability and the presence of residual oxygen in the chamber atmosphere, which favors the formation of Mo–O bonds under high-temperature conditions [18]. The emergence of MoO_2 is undesirable for electronic and thermoelectric applications, as this oxide phase introduces defect levels that reduce carrier mobility and degrade functional performance [19].

For the Ag-doped film (J3), two additional peaks were observed at 2θ ≈ 28.0° and 2θ ≈ 44.3°, corresponding to $AgNO_3$ and metallic Ag, respectively, confirming successful incorporation of Ag species during deposition. The presence of metallic Ag suggests partial thermal decomposition of $AgNO_3$ during PVD, consistent with previously reported Ag–MoS_2 composite films, where Ag nanoparticles modify the local electronic environment and increase carrier concentration [20]. These compositional features are relevant for thermoelectric applications, where noble metal doping has been shown to enhance the Seebeck coefficient while reducing lattice thermal conductivity [21].

In all samples, an additional intense diffraction peak at 2θ ≈ 69.1° was observed. This reflection corresponds to the Si(400) plane of the crystalline silicon substrate (Cu Kα radiation). Since the thermally grown SiO_2 layer (~280 nm) is amorphous, it does not generate Bragg reflections, allowing the substrate peak to remain prominent. This peak is now explicitly labeled in Figure 3 to avoid misinterpretation.

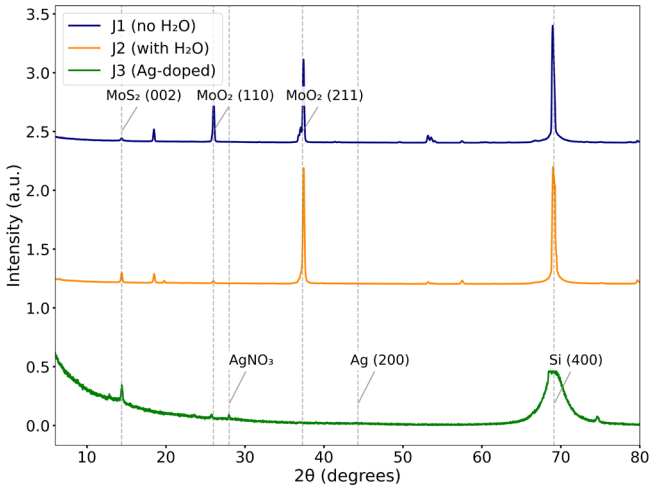

Figure 3. X-ray diffraction (XRD) patterns of samples J1, J2, and J3. The diffractograms show the characteristic MoS_2 (002) peak in all samples, confirming film formation. The Si(400) substrate peak is also present in all measurements. For samples J1 and J2, additional peaks associated with MoO_2 [(110) and (211)] are observed, while sample J3 exhibits extra peaks attributed to $AgNO_3$ and Ag(200), resulting from silver doping. The curves were vertically offset to facilitate comparison among the patterns.

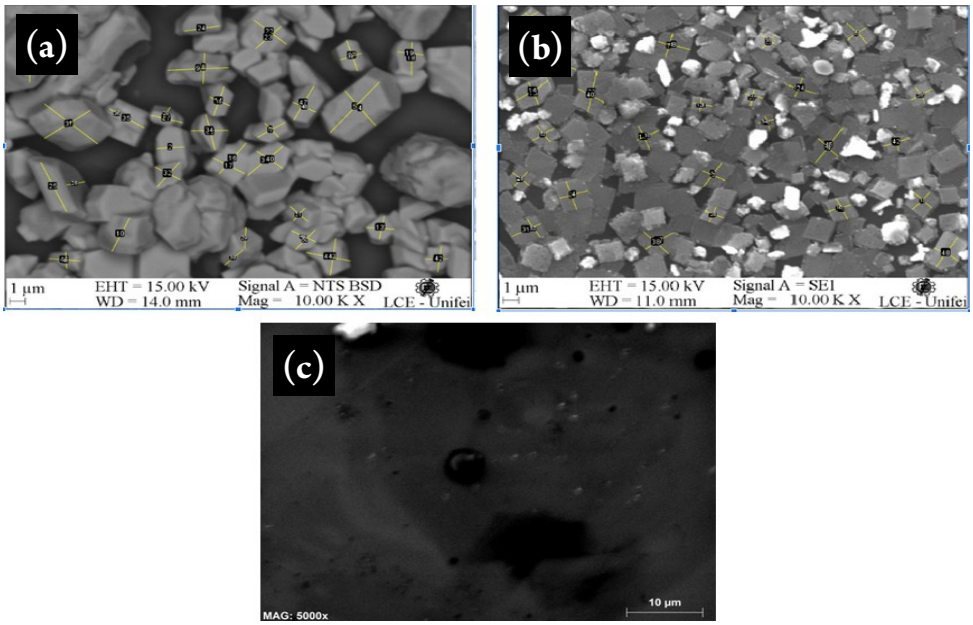

Figure 4. SEM micrographs of MoS_2 thin films: (a) sample J1 (no H_2O), showing irregular grain distribution and incomplete coalescence; (b) sample J2 (with H_2O), exhibiting smoother surfaces and improved grain uniformity; and (c) sample J3 (Ag-doped), displaying densely packed spherical grains and enhanced film compactness.

The combined analysis of the three diffractograms highlights the beneficial effect of water vapor as a mild reducing and growth-directing agent that suppresses oxidation and promotes crystalline MoS_2 formation (J2), while Ag incorporation (J3) introduces additional crystalline phases that can modulate charge transport and electronic structure. These structural differences directly correlate with the Raman and morphological results presented in the following sections, further demonstrating how controlled variations in the synthesis environment can significantly influence the final quality of MoS_2 thin films.

Figure 4(a–c) presents the SEM micrographs of samples J1, J2, and J3, respectively, allowing a direct comparison of the morphological evolution induced by H_2O-assisted growth and Ag incorporation. In Figure 4(a), corresponding to sample J1, the film exhibits a heterogeneous surface with irregular grain shapes, nonuniform grain distribution, and significant variations in intergranular spacing. These morphological irregularities indicate limited adatom mobility during deposition, leading to incomplete coalescence and higher porosity, conditions typically associated with MoS_2 growth under restricted surface diffusion.

In Figure 4(b), representing sample J2 synthesized in the presence of H_2O vapor, a more uniform and compact morphology is observed. The grains exhibit smoother surfaces, reduced voids, and more coherent grain boundary networks. This densification is consistent with the enhanced crystallinity revealed by XRD and aligns with the findings of Macha et al. [22] and Cai et al. [23], who showed that controlled H_2O introduction promotes nucleation and surface diffusion during TMD film growth.

Figure 4(c), corresponding to sample J3 doped with Ag, displays a distinctive morphology composed of densely packed, nearly spherical grains with minimal variation in size. The incorporation of Ag leads to a more continuous and fully coalesced microstructure, with significantly improved grain connectivity. This is advantageous for electronic and thermoelectric applications, as it reduces grain-boundary resistance and enhances charge-transport pathways. Similar improvements in densification and connectivity have been reported in noble-metal-doped MoS_2 films [25].

The SEM results show a clear morphological progression: J1 exhibits incomplete grain coalescence, J2 demonstrates improved uniformity due to water-assisted synthesis, and J3 achieves the highest level of densification as a result of Ag incorporation.

The grain size distributions of samples J1, J2, and J3 are presented in Figure 5. Sample J1 exhibits an average grain size of 2.34 ± 1.04 µm, with a relatively broad distribution that reflects the irregular and partially coalesced morphology observed in the SEM images. In contrast, sample J2 (Figure 5(b)) shows a significantly smaller and more uniform average grain size of 1.28 ± 0.58 µm, consistent with the densifying effect of water-assisted growth. The reduced grain size in J2 also implies increased phonon scattering, which is known to decrease lattice thermal conductivity in layered materials [24].

Sample J3 (Figure 5 (c)), synthesized with Ag incorporation, displays a distinct behavior, with an average grain size of 5.14 ± 2.97 µm. The considerably larger grains and wider distribution indicate that silver doping modifies the growth dynamics, favoring coarsening and the formation of more interconnected microstructures. This agrees with the SEM results, where J3 shows compact and well-connected grains, likely supported by Ag-induced changes in surface energy and nucleation density.

These microstructural differences are relevant for thermoelectric performance. Smaller and more uniformly distributed grains (as in J2) enhance phonon scattering and can reduce thermal conductivity [24], while larger grains with improved connectivity (as in J3) tend to lower grain-boundary resistance and favor charge

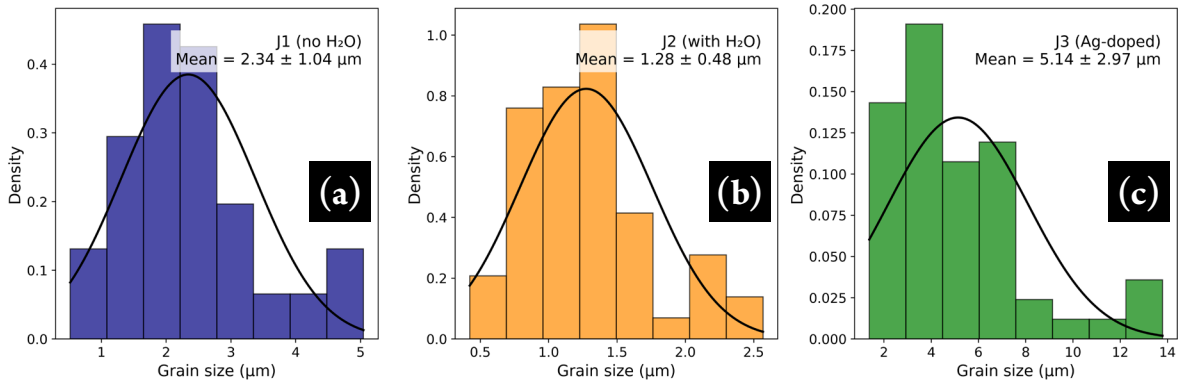

Figure 5. Grain size histograms of MoS_2 thin films: (a) J1, (b) J2, and (c) J3. J1 exhibits a broad distribution centered at 2.34 ± 1.04 μm. J2 shows a narrower and more uniform distribution (1.28 ± 0.58 μm), while J3 presents the largest grains (5.14 ± 2.97 μm), consistent with Ag-modified growth kinetics.

transport. Thus, each film offers different trade-offs depending on whether electrical conductivity or thermal suppression is prioritized.

Raman spectroscopy results (Figure 6) provided complementary information about the crystallinity and oxidation state of the films. For sample J1, a single prominent peak at 385 cm^{-1} (E_2g^1 mode) was observed, while the A_1g mode (~411 cm^{-1}) was absent, indicating defective crystallinity. Additional peaks near 344 and 360 cm^{-1} correspond to Mo–O vibrations, confirming the presence of MoO_2 [9]. Conversely, the Raman spectrum of J2 exhibited both E_2g^1 and A_1g modes with a frequency difference of approximately 26 cm^{-1}, characteristic of few-layer MoS_2 [26]. The absence of Mo–O-related peaks reinforces that H_2O-assisted growth suppressed oxidation. For the Ag-doped sample (J3), a slight redshift (~1–2 cm^{-1}) of the vibrational modes was detected, attributed to local strain and electron–phonon coupling induced by Ag incorporation [27].

The structural and vibrational differences observed among samples J1, J2, and J3 are directly relevant to the photoelectric behavior of MoS_2. As a layered semiconductor, MoS_2 exhibits strong light–matter interactions and photoconductive response, which are sensitive to crystallinity, defect density, and local strain. The improved crystallinity and reduced oxidation observed in sample J2 are expected to enhance carrier mobility and suppress non-radiative recombination, thereby improving optoelectronic performance. In contrast, the partial formation of MoO_2 in sample J1 introduces mid-gap states that tend to trap photogenerated carriers, degrading photoresponse. For the Ag-doped film (J3), the Raman redshift and the presence of Ag species suggest modified charge distribution and enhanced electron–phonon coupling, which can facilitate charge separation under illumination and potentially improve photoconductive gain. Although photoelectric measurements were not performed in this work, the structural findings provide insight into how synthesis parameters modulate properties relevant to optoelectronic applications.

The EDS results (Figures 7–8) confirmed the presence of Mo, S, Si, and O in samples J1 and J2, consistent with MoS_2 deposited on a SiO_2 substrate. In Figure 9, the presence of Mo, Si, and O was also detected; however, the Ag-doped film (J3) exhibited an additional silver signal (≈0.11 wt%), thereby confirming the successful doping. The controlled Ag incorporation likely altered the local electronic environment without forming unwanted large metallic aggregates, as corroborated by the absence of secondary silver clusters in SEM images. Such dopant incorporation can enhance Seebeck coefficients and electrical conductivity, as observed in other Ag–MoS_2 systems [28].

To complement the structural and morphological characterization, Energy-Dispersive X-ray Spectroscopy (EDS) was performed on samples J1, J2, and J3 to quantitatively evaluate their elemental composition. This analysis provides insight into the effects of water vapor and Ag incorporation on the chemical makeup of the MoS_2 films, particularly regarding oxidation level, sulfur content, and dopant incorporation.

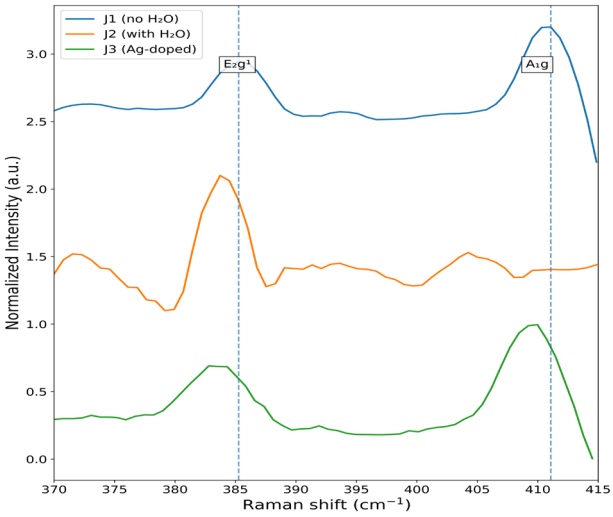

Figure 6. Raman spectra of MoS_2 thin films synthesized under different conditions: J1 (no H_2O), J2 (with H_2O), and J3 (Ag-doped). The characteristic MoS_2 vibrational modes E_2g^1 and A_1g are highlighted, showing improved crystallinity for sample J2 and a redshift of both modes in sample J3 due to strain effects and electron–phonon coupling induced by Ag incorporation. Spectra are vertically offset for clarity.

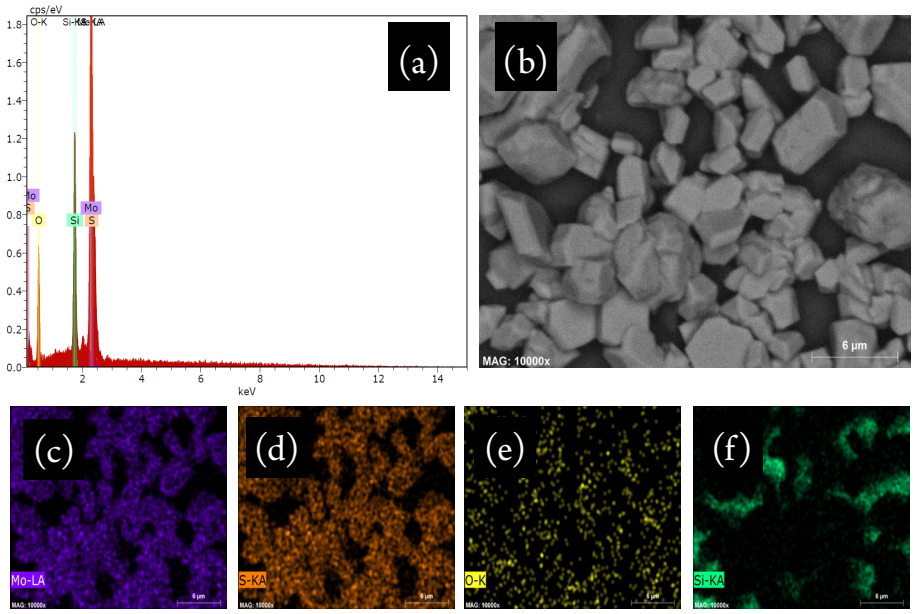

Figure 7. (a) Histogram, (b) micrograph and (c) - (f) chemical composition images obtained by SEM-EDS of sample J1.

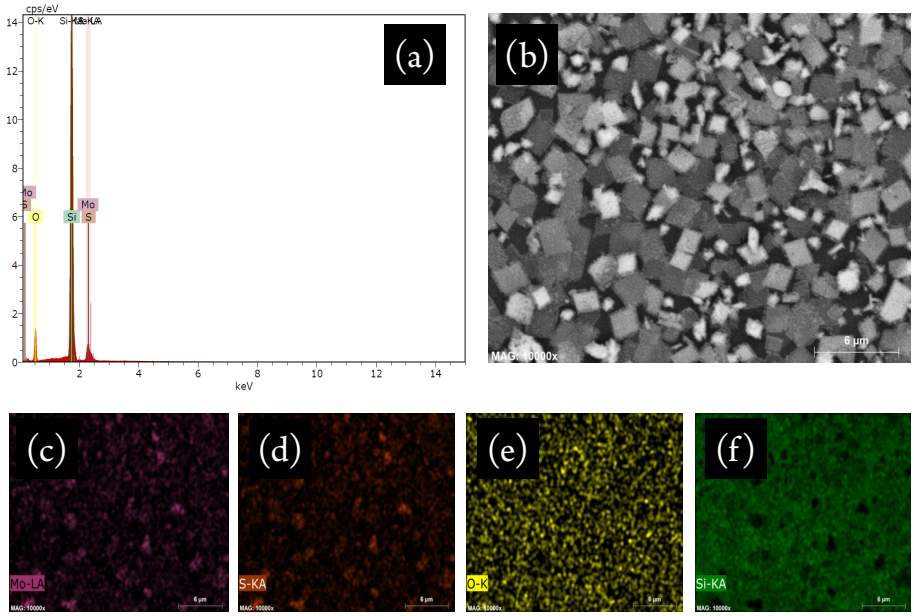

Figure 8. (a) Histogram, (b) micrograph and (c) - (f) chemical composition images obtained by SEM-EDS of sample J2.

The quantitative EDS results provide a deeper understanding of the chemical composition of the MoS_2 films. Sample J1 shows high oxygen content and a Mo-rich composition, confirming the presence of MoO_2, in agreement with the XRD findings. Sample J2, synthesized in the presence of H_2O vapor, exhibits reduced oxidation and a more uniform elemental distribution, consistent with the improved crystallinity observed in XRD and Raman analyses. In turn, sample J3 presents clear evidence of Ag incorporation, although the Mo signal appears low due to its island-like growth morphology, which limits the interaction volume of the electron beam with the MoS_2 phase.

These quantitative findings reinforce and support the structural, vibrational, and morphological results discussed throughout the manuscript. The normalized weight and atomic percentages obtained from EDS are summarized in Table 1.

The structural and morphological differences observed among the samples also have relevant implications for thermoelectric transport. The enhanced crystallinity and reduced oxidation detected in J2 favor phonon suppression and long-range carrier mobility, whereas the improved grain connectivity and compact morphology of the Ag-doped film (J3) are expected to reduce grain-boundary scattering and increase electrical

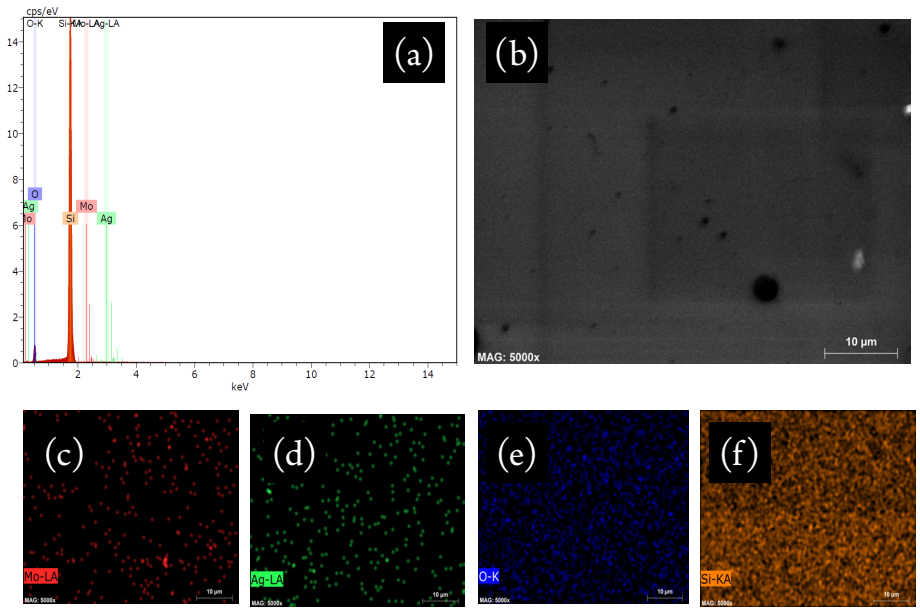

Figure 9. (a) Histogram, (b) micrograph and (c) - (f) chemical composition images obtained by SEM-EDS of sample J3.

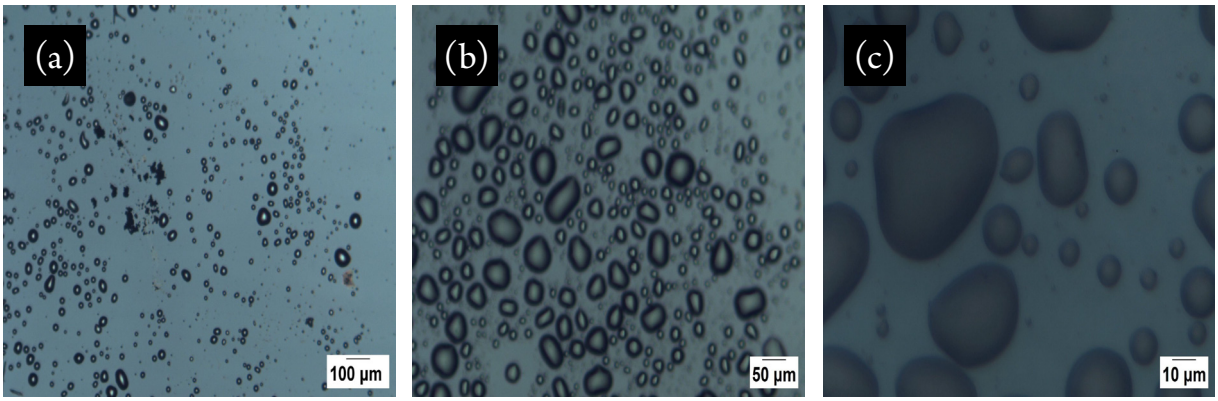

Figure 10. Optical microscopy images of MoS_2 thin films: (a) J1 (no H_2O), showing contrast variations and irregular domains; (b) J2 (with H_2O), exhibiting more homogeneous surface texture and improved uniformity; and (c) J3 (Ag-doped), featuring dome-like bright regions associated with Ag-induced surface reorganization.

Table 1. Quantitative EDS composition and discussion.

Sample	Element	Norm. wt %	Atom %	Interpretation
J1	O	31.53	65.55	High Oxygen MoO_2 formation
	S	2.17	2.25	Low sulfur content
	Mo	55.30	19.17	Mo-rich/oxidation
	Si	64.90	60.28	Dominant substrate
J2	S	0.67	0.54	Low but uniform S
	Mo	12.49	3.39	Thin MoS_2 layer
	Si	84.62	76.12	Substrate due to island growth
	O	15.07	23.80	Moderate oxidation
J3	Mo	0.20	0.05	Very low Mo signal
	Ag	0.11	0.03	Confirms Ag incorporation

conductivity. In contrast, the higher defect density and incomplete coalescence observed in J1 likely limit charge-carrier pathways and degrade thermoelectric efficiency. Although full thermoelectric measurements were not performed in this study, the combined XRD, SEM, and Raman results already provide clear indicators of which growth conditions are more favorable for charge-transport-based applications.

Figure 10(a–c) presents the optical microscopy images of samples J1, J2, and J3, respectively. In Figure 10(a), corresponding to J1, the film shows irregular contrast variations, nonuniform domains, and local thickness fluctuations. These features indicate incomplete surface coverage and heterogeneous growth, consistent with the irregular grain distribution observed in SEM and with the presence of MoO_2 detected by XRD.

Figure 10(b), referring to sample J2 synthesized under H_2O vapor, displays a much more uniform optical response, with smoother contrast distribution and fewer defect-like regions. The improved homogeneity reflects enhanced layer formation and

reduced porosity, corroborating the densification and crystallinity improvements indicated by XRD and SEM analyses.

Figure 10(c), corresponding to the Ag-doped sample J3, reveals prominent dome-like and circular bright structures distributed across the surface. These three-dimensional features are indicative of localized vertical growth, strain relaxation, and dopant-induced nucleation mechanisms. Such dome-like morphologies have been reported in MoS_2 and related TMDs as signatures of exciton confinement and enhanced light absorption. Their presence suggests that Ag incorporation influences surface energy and growth kinetics, consistent with the compact grain morphology observed in SEM and the Raman redshift attributed to Ag-induced strain effects.

The optical microscopy results complement the structural and vibrational analyses, highlighting the distinct growth behaviors of J1, J2, and J3 and the strong influence of H_2O vapor and Ag doping on the surface evolution of MoS_2 thin films.

4. CONCLUSION

This study investigated the influence of synthesis conditions on the structural and compositional properties of molybdenum disulfide (MoS_2) thin films deposited on SiO_2 substrates by Physical Vapor Deposition (PVD). The X-ray diffraction (XRD) results demonstrated that the introduction of water vapor during synthesis favored the formation of crystalline MoS_2, evidenced by the enhanced intensity of the (002) reflection and suppression of the MoO_2 phase. These findings indicate that controlled water addition acts as a growth enhancer, improving crystallinity and reducing oxidation.

For the Ag-doped sample (J3), the XRD patterns revealed well-defined peaks corresponding to MoS_2, metallic silver (Ag), and silver nitrate ($AgNO_3$), with nanometric crystallite sizes indicative of a nanocrystalline morphology. Scanning Electron Microscopy (SEM) confirmed the formation of spherical, densely packed grains, enhancing intergranular connectivity and potentially facilitating charge transport. Energy-Dispersive X-ray Spectroscopy (EDS) analysis confirmed the successful and controlled incorporation of silver, while optical microscopy revealed dome-shaped features associated with vertical growth, suggesting significant morphological reorganization induced by Ag doping.

The results collectively confirm that both water-assisted synthesis and Ag incorporation play decisive roles in determining the crystallinity, oxidation state, and surface morphology of MoS_2 thin films. Water promotes improved structural order and phase purity, whereas silver doping modifies surface morphology and may enhance carrier mobility by introducing additional electronic states and improving inter-grain contact. The ability to control these parameters is crucial for optimizing the performance of MoS_2 films in functional devices.

In particular, the MoS_2 film synthesized in the presence of H_2O (sample J2) exhibited superior crystallinity and minimal oxidation, confirmed by Raman analysis, demonstrating its potential for use in optoelectronic and thermoelectric devices. Meanwhile, the compact and homogeneous morphology observed in the Ag-doped sample (J3) suggests suitability for applications in field-effect transistors (FETs), gas sensors, photodetectors, and thermoelectric generators, where carrier mobility and structural stability are key factors.

These structural differences also have important implications for optoelectronic applications, since MoS_2 is known for its strong photoelectric response. The enhanced crystallinity of J2 and the modified electronic environment induced by Ag in J3 are expected to support improved photogenerated carrier transport, while the oxidation observed in J1 would adversely affect photoresponse. Thus, even though photoelectric characterization was beyond the scope of the present study, the results presented here provide useful guidelines for tailoring the optical and electronic properties of PVD-grown MoS_2 films.

Future work should focus on correlating the structural modifications observed here with electrical and thermoelectric performance through measurements of conductivity, Seebeck coefficient, and carrier concentration. Additional studies on the thermal and chemical stability of the films under various environmental conditions are also recommended. Furthermore, systematic variation of synthesis parameters, such as gas flow rate, sulfur-to-metal ratio, and temperature profile, could yield valuable insights into the optimization of MoS_2-based materials for targeted energy conversion and sensing applications.

Although complete thermoelectric measurements were not included in the present study due to the lack of specialized instrumentation, we acknowledge their importance and plan to incorporate Seebeck coefficient and electrical conductivity tests in future work. These assessments will enable a direct correlation between the structural and morphological findings reported here and the actual energy-conversion performance of the MoS_2 thin films.

ACKNOWLEDGEMENTS

The authors would like to express their gratitude for the financial support from the Minas Gerais Research Foundation (FAPEMIG – Grant APQ-03495-25 and Grant APQ-00620-23), the National Council for Scientific and Technological Development (CNPq), and the Coordination for the Improvement of Higher Education Personnel (CAPES). A special thanks is also extended to the Interdisciplinary Laboratory for Characterization, Innovation, and Development (LInCaDI), where the experimental work was carried out.

CREDIT AUTHOR STATEMENT

Joede dos Passos: Conceptualization, Methodology, Investigation, Data Curation, Formal Analysis, Visualization, Writing – Original Draft. **Adhimar Flavio Oliveira**: Supervision, Conceptualization, Methodology, Writing – Review & Editing, Validation, Resources. **Rero Marques Rubinger**: Supervision, Funding Acquisition, Resources, Project Administration, Writing – Review & Editing.

DECLARATIONS

Conflict of interest The authors declare that they have no known competing financial interests or personal relationships that could have appeared to influence the work reported in this paper.

REFERENCES

[1] Ismail, K. B. M., Arun Kumar, M., Mahalingam, S., Kim, J., & Atchudan, R. (2023). Recent advances in molybdenum disulfide and its nanocomposites for energy applications: Challenges and development. Materials, 16(12), 4471.

[2] Lei, Z., Zhan, J., Tang, L., Zhang, Y., & Wang, Y. (2018). Recent development of the metallic (1T) phase of molybdenum disulfide for energy conversion and storage. Advanced Energy Materials, 8(19), 1703482.

[3] Zhu, Y., Lim, J., Zhang, Z., Wang, Y., Sarkar, S., Ramsden, H., ... & Chhowalla, M. (2023). Room-temperature photoluminescence mediated by sulfur vacancies in 2D molybdenum disulfide. ACS nano, 17(14), 13545-13553.

[4] Zhou, Z., Li, X., Hu, T., Xue, B., Chen, H., Ma, L., ... & Tan, C. (2022). Molybdenum-based nanomaterials for photothermal cancer therapy. Advanced NanoBiomed Research, 2(11), 2200065.

[5] Chen, F., Luo, Y., Liu, X., Zheng, Y., Han, Y., Yang, D., & Wu, S. (2022). 2D molybdenum sulfide-based materials for photo-excited antibacterial application. Advanced Healthcare Materials, 11(13), 2200360.

[6] Muratore, C., Voevodin, A. A., & Glavin, N. R. (2019). Physical vapor deposition of 2D Van der Waals materials: a review. Thin Solid Films, 688, 137500.

[7] Hao, Najmaei, S., Yuan, J., Zhang, J., Ajayan, P., & Lou, J. (2015). Synthesis and defect investigation of two-dimensional molybdenum disulfide atomic layers. Accounts of Chemical Research, 48(1), 31-40.

[8] Zhou, W., Zou, X., Najmaei, S., Liu, Z., Shi, Y., Kong, J., ... & Idrobo, J. C. (2013). Intrinsic structural defects in monolayer molybdenum disulfide. Nano letters, 13(6), 2615-2622.

[9] Ge, H., Kuwahara, Y., & Yamashita, H. (2022). Development of defective molybdenum oxides for photocatalysis, thermal catalysis, and photothermal catalysis. Chemical Communications, 58(61), 8466-8479.

[10] Yin, W., Yu, J., Lv, F., Yan, L., Zheng, L. R., Gu, Z., & Zhao, Y. (2016). Functionalized nano-MoS2 with peroxidase catalytic and near-infrared photothermal activities for safe and synergetic wound antibacterial applications. ACS nano, 10(12), 11000-11011.

[11] Wu, P., Yin, N., Li, P., Cheng, W., & Huang, M. (2017). The adsorption and diffusion behavior of noble metal adatoms (Pd, Pt, Cu, Ag and Au) on a MoS 2 monolayer: a first-principles study. Physical Chemistry Chemical Physics, 19(31), 20713-20722.

[12] Li, Z., Zhou, D. A., & Xiangke, J. (2021). Highly selective adsorption on monolayer MoS2 doped with Pt, Ag, Au and Pd and effect of strain engineering: A DFT study. Sensors and Actuators A: Physical, 322, 112637.

[13] Li, X., Wang, T., Jiang, F., Liu, J., Liu, P., Liu, G., ... & Jiang, Q. (2019). Optimizing thermoelectric performance of MoS2 films by spontaneous noble metal nanoparticles decoration. Journal of Alloys and Compounds, 781, 744-750.

[14] Baaalla, N., Absike, H., Mezzat, F., Hlil, E. K., Masrour, R., Benyoussef, A., & El Kenz, A. (2024). Insights into Ag2Mo3SeO12 for photovoltaic and optoelectronic applications: a theoretical exploration of its structural, electronic, and thermoelectric behavior. Materials Today Chemistry, 40, 102267.

[15] Zaccaro, S. J. V., Oliveira, A. F., Rubinger, R. M., de Siqueira, C. C., & da Costa Junior, R. A. (2021). Determination of thickness and refractive index of SiO2 thin films using the cross-entropy global optimization method. Research, Society and Development, 10(10), e326101019028-e326101019028.

[16] Manikandan, R., & Raina, G. (2022). Hydrothermally synthesized 2H-MoS2 under optimized conditions–A structure and morphology analysis. Physica Scripta, 97(12), 125808.

[17] Jin, Y., Cheng, M., Liu, H., Ouzounian, M., Hu, T. S., You, B., ... & Liu, S. (2020). Na2SO4-regulated high-quality growth of transition metal dichalcogenides by controlling diffusion. Chemistry of Materials, 32(13), 5616-5625.

[18] Szoszkiewicz, R. (2021). Local interactions of atmospheric oxygen with MoS2 crystals. Materials, 14(20), 5979.

[19] Shalini, V., Harish, S., Ikeda, H., Hayakawa, Y., Archana, J., & Navaneethan, M. (2023). Investigating the effect of defect states and to enhance the electrical conductivity of p-type Vanadium-doped MoS2 for wearable thermoelectric application. Journal of Alloys and Compounds, 960, 170317.

[20] Tan, S. Y., Yen, H. M., Leong, K. L., Ong, W., & Lim, J. X. (2022, March). Synthesis of Graphene/Silver/Molybdenum Disulphide Composite for Supercapacitor Application. In Materials Science Forum (Vol. 1054, pp. 21-30). Trans Tech Publications Ltd.

[21] Khoshab, M., Iranmanesh, P., & Saeednia, S. (2024). Biocompatible synthesis of MoS2/Ag nanocomposite for enhanced photocatalytic activity via surface plasmon effects. Applied Physics A, 130(11), 828.

[22] Macha, M., Zhao, Z., Kang, K., Cho, Y., Kim, D., & Jeon, J. (2022). Wafer-scale MoS_2 with water-vapor-assisted showerhead MOCVD. Nanoscale Advances, 4(17), 4391–4401. https://doi.org/10.1039/D2NA00409G.

[23] Cai, Q., Wang, X., Zhang, Y., Li, X., Zhang, J., & Pan, C. (2022). Water-assisted growth of two-dimensional $MoS_2/MoSe_2$ vertical heterostructures on molten glass. Nanoscale, 14(6), 1990–1996. https://doi.org/10.1039/D1NR08095D.

[24] Chen, D., Chen, H., Hu, S., Guo, H., Sharshir, S. W., An, M., ... & Zhang, X. (2020). Influence of atomic-scale defect on thermal conductivity of single-layer MoS2 sheet. Journal of Alloys and Compounds, 831, 154875.

[25] Inwati, G. K., Yadav, V. K., Ali, I. H., Kakodiya, S. D., Choudhary, N., Makwana, B. A., ... & Cavalu, S. (2022). Enhanced plasmon based Ag and Au nanosystems and their improved biomedical impacts. Crystals, 12(5), 589.

[26] Rout, C. S., & Late, D. J. (2022). Raman Spectroscopy-Based Techniques for 2D Layered Materials. Advanced analytical techniques for characterization of 2D materials.

[27] Rani, E., Gupta, V. K., Thasfiquzzaman, M., Talebi, P., Martinelli, A., Niu, Y., ... & Cao, W. (2022). Unraveling compensation between electron transfer and strain in Ni-Ag-MoS2 photocatalyst. Journal of Catalysis, 414, 199-208.

[28] Shalini, V., Harish, S., Ikeda, H., Hayakawa, Y., Archana, J., & Navaneethan, M. (2023). Investigating the effect of defect states and to enhance the electrical conductivity of p-type Vanadium-doped MoS2 for wearable thermoelectric application. Journal of Alloys and Compounds, 960, 170317.